Study of selected benzyl azides by UV photoelectron spectroscopy and mass spectrometry

R.M. Pinto [a], R.I. Olariu [b], J. Lameiras [c], F.T. Martins [c,1], A.A. Dias [a], G.J. Langley [d], P. Rodrigues [e], C.D. Maycock [e,f], J.P. Santos [a], M.F. Duarte [c], M.T. Fernandez [c], M.L. Costa [a,*]

[a] CFA, Centro de Física Atómica, Departamento de Física, Faculdade de Ciências e Tecnologia, FCT, Universidade Nova de Lisboa, 2829-516 Caparica, Portugal
[b] Department of Analytical Chemistry, "Al. I. Cuza" University of Iasi, 11 Carol I Bd., 700506 Iasi, Romania
[c] CQB, Centro de Química e Bioquímica, Departamento de Química e Bioquímica, Faculdade de Ciências da Universidade de Lisboa, Campo Grande, 1749-016 Lisboa, Portugal
[d] School of Chemistry, University of Southampton, Highfield, Southampton SO17 1BJ, UK
[e] ITQB, Instituto de Tecnologia Química e Biológica, Universidade Nova de Lisboa, Apartado 127, 2780-901 Oeiras, Portugal
[f] Departamento de Química e Bioquímica, Faculdade de Ciências da Universidade de Lisboa, Campo Grande, 1749-016 Lisboa, Portugal

ARTICLE INFO

ABSTRACT

Benzyl azide and the three methylbenzyl azides were synthesized and characterized by mass spectrometry (MS) and ultraviolet photoelectron spectroscopy (UVPES). The electron ionization fragmentation mechanisms for benzyl azide and their methyl derivatives were studied by accurate mass measurements and linked scans at constant B/E. For benzyl azide, in order to clarify the fragmentation mechanism, labelling experiments were performed. From the mass analysis of methylbenzyl azides isomers it was possible to differentiate the isomers *ortho*, *meta* and *para*. The abundance and nature of the ions resulting from the molecular ion fragmentation, for the three distinct isomers of substituted benzyl azides, were rationalized in terms of the electronic properties of the substituent. Concerning the *para*-isomer, IRC calculations were performed at UHF/6-31G(d) level. The photoionization study of benzyl azide, with He(I) radiation, revealed five bands in the 8–21 eV ionization energies region. From every photoelectron spectrum of methylbenzyl azides isomers it has been identified seven bands, on the same range as the benzyl azide. Interpretation of the photoelectron spectra was accomplished applying Koopmans' theorem to the SCF orbital energies obtained at HF/6-311++G(d, p) level.

© 2010 Elsevier B.V. All rights reserved.

1. Introduction

Phenyl azide prepared in the nineteenth century was the first synthetic organic azide [1]. Since then the application of organic azides, in science and technology, has grown dramatically [1–3]. Organic azides have been largely used as precursors for synthesis [1–3], for amines and recently in "click" chemistry [4–7]. This concept has, recently, emerged [4] exploiting rapid, modular reactions developing under a large thermodynamic driving force. The resulting synthetic products have been applied in areas such as supramolecular chemistry [5], biochemistry [6] and in developing compounds relevant for antiviral and anticancer treatment [7]. On the other hand, azidonucleosides showed to be of primordial interest in AIDS treatment [2,8], azido sugars in biological labelling [9] and in tumor-growth inhibition [10]. Moreover, azides are potential high-energy density materials (HEDMs) [11] and are also used in the generation of electrically conducting polymers [12] and in the covalent modification of polymer surfaces [13].

Due to their thermodynamic instability, explosive nature and shock sensitivity [11], their structural characterization is experimentally challenging. However, the physico-chemical properties of some aliphatic azides have been investigated spectroscopically by ultraviolet photoelectron spectroscopy (UVPES) and matrix isolation infrared spectroscopy (MIIS) [14–16]. Electron ionization mass spectrometry (EIMS) has been successfully applied to the study of phenyl azides and its derivatives [17]. Some azides, already studied by UVPES and MIIS were also investigated by EIMS [18,19] and chemical ionization mass spectrometry (CIMS) [20].
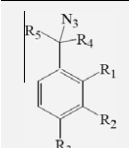
At present very little is known about the fate of organic azides involving an aromatic ring such as benzyl azide. Thus, benzyl azide and three methylated isomers were synthesized and characterized in terms of electronic configuration and ionization energies, using mass spectrometry and UV photoelectron spectroscopy.

Table 1
Structures of the studied benzyl azides.

	Compound	R_1	R_2	R_3	R_4	R_5
	1	H	H	H	H	H
	2	H	H	H	D	D
	3	CH_3	H	H	H	H
	4	H	CH_3	H	H	H
	5	H	H	CH_3	H	H

The present paper reports a combined experimental study of the following compounds shown in Table 1: benzyl azide (BA) (**1**), deuterated benzyl azide (**2**), 2-methylbenzyl azide (2-MBA) (**3**), 3-methylbenzyl azide (3-MBA) (**4**), 4-methylbenzyl azide (4-MBA) (**5**). Experimental results were supported by theoretical calculations.

2. Experimental and theoretical methods

2.1. General procedure for sample preparation and characterization

The azides are potentially explosive and therefore must be handled with all due precautions. Azides and some decomposition products like HCN may be toxic [21].

Sodium azide (2 equiv.) was added slowly to a solution of the appropriate benzyl halide in dimethyl sulfoxide. The mixture was stirred at room temperature until TLC analysis (hexane:dichloromethane 7:3) indicated completion of the reaction. The mixture was quenched with distilled water, extracted with diethyl ether and the combined organic phases were dried over anhydrous sodium sulphate, filtered and concentrated [22]. After preparative TLC the product obtained ($\eta > 90\%$) was analyzed by FTIR (Mattson Satellite-FITR) and by NMR (Bruker ARX400). The deuterated benzyl azide was prepared under argon from benzyl bromide-α,α-d$_2$ in deuterium oxide.

Care was taken to minimize the effect of possible explosions at all stages in the preparation and handling of the azide samples, but no untoward occurrences were experienced during this work. The products were characterized in the vapour phase by UV photoelectron spectroscopy and mass spectrometry and in the liquid phase by ^{1}H and ^{13}C NMR and by IR spectroscopy.

Benzyl azide (**1**): IR data (neat): ν_{max}2098 (N$_3$) cm^{-1}; ^{1}H NMR data (400 MHz, CDCl$_3$): δ 4.35 (s, CH$_2$), 7.34–7.44 (m, CH arom.) ppm; ^{13}C NMR data (100 MHz, CDCl$_3$): δ 54.7 (CH$_2$), 128.2–128.8, 135.3 ppm.

Deuterated benzyl azide (**2**): IR data (neat): ν_{max} 2100 (N$_3$) cm^{-1}; ^{1}H NMR data (400 MHz, CDCl$_3$): δ 7.25–7.41 (m, CH arom.) ppm; ^{13}C NMR data (100 MHz, CDCl$_3$): δ 128.2–128.8, 135.3 ppm.

2-Methylbenzyl azide (**3**): IR data (neat): ν_{max} 2096 (N$_3$) cm^{-1}; ^{1}H NMR data (400 MHz, CDCl$_3$): δ 2.35 (CH$_3$), 4.32 (s, CH$_2$), 7.18–7.26 (m, CH arom.) ppm; ^{13}C NMR data (100 MHz, CDCl$_3$): δ 18.9 (CH$_3$), 53.0 (CH$_2$), 126.2, 128.6, 129.3, 130.6, 133.3, 136.7 ppm.

3-Methylbenzyl azide (**4**): IR data (neat): ν_{max} 2096 (N$_3$) cm^{-1}; ^{1}H NMR data (400 MHz, CDCl$_3$): δ 2.39 (CH$_3$), 4.32 (s, CH$_2$), 7.13–7.32 (m, CH arom.) ppm; ^{13}C NMR data (100 MHz, CDCl$_3$): δ 21.3 (CH$_3$), 54.8 (CH$_2$), 125.2, 128.7, 128.9, 129.0, 135.3, 138.5 ppm.

4-Methylbenzyl azide (**5**): IR data (neat): ν_{max} 2098 (N$_3$) cm^{-1}; ^{1}H NMR data (400 MHz, CDCl$_3$): δ 2.35 (CH$_3$), 4.27 (s, CH$_2$), 7.17–7.23 (m, CH arom.) ppm; ^{13}C NMR data (100 MHz, CDCl$_3$): δ 21.1 (CH$_3$), 54.6 (CH$_2$), 128.2, 129.5, 132.3, 138.1 ppm.

2.2. Mass spectrometry

The electron ionization (EI) mass spectrometry technique was used to undertake all the mass spectra presented herein by using an AEI-MS9 mass spectrometer updated by VG Analytical Instruments. Electron ionization mass spectrometry was performed with nominal electron energies of 70 eV, 200 mA trap current, and a source housing pressure of about 1.33×10^{-4} Pa and analyser pressure about 2.66×10^{-5} Pa. The ions were accelerated through 8 kV. Linked scans at constant B/E were also accomplished for all important fragmentation peaks identified in the normal mass spectra. For some of the ions, high resolution accurate mass data, were obtained using a VG70-250SE mass spectrometer with resolution of 10,000 (10% valley) by the peak matching technique with perfluorokerosene (PFK) as a reference compound.

2.3. Photoelectron spectroscopy

The photoelectron (PE) spectra obtained for benzyl azide and its methyl derivatives were recorded using the single detector instrument described elsewhere [23]. All the aromatic azides investigated herein were liquid with a relatively sufficient vapour pressure at room temperature to allow PE spectra to be recorded with acceptable signal-to-noise ratio. The spectra were obtained by direct pumping on a liquid sample held in a small flask through a needle valve outside the spectrometer ionization chamber. The operating resolution of the photoelectron spectrometer was typically 30 meV as measured for argon (3p)$^{-1}$ fwhm ionized with He(I)α radiation (21.22 eV).

Calibration of the vertical ionization energies (VIEs) of the parent azides photoelectron bands was achieved using argon and methyl iodide [24] added to the ionization chamber at the same time as the azide vapour samples. PE spectra were obtained for the starting materials used in the preparation of the studied samples. No evidence of bands associated with starting materials was found in PE spectra recorded for purified samples of the azides under study.

2.4. Computational details

All theoretical calculations were carried out with the Gaussian 03 program package [25]. Full structure optimization was performed on each molecule, with the Hartree–Fock (HF) method and the 6-311++G(d,p) basis [26], to establish equilibrium geometries, and subsequently to calculate VIEs. The starting geometries for all optimizations were the ones obtained in a previous conformational study and already correspond to lowest energy geometries [27].

For the VIEs, Koopmans' theorem [28] was applied to the SCF orbital energies obtained at HF/6-311++G(d,p) level. The computed molecular orbitals (MOs) energies ϵ_i of benzyl azide and its methyl derivatives were assigned to the experimental ionization energies obtained in the spectra, as IE$_i \approx -\epsilon_i$, in a non-scaled form.

In order to support the mass spectrometry studies, the optimized geometries of the radical cations of benzyl azide (BA), 2-, 3- and 4-methylbenzyl azide (2-, 3- and 4-MBA) were obtained at the UHF/6-311++G(d,p) level of theory. Furthermore, in order to support some fragmentation pathways concerning 4-MBA, an initial search for the transition structures (TS) connecting the precursor and the product ions was performed by scanning the length of a particular bond of interest and optimizing the remaining structural parameters. The TS existence was verified by full optimization of its geometry, followed by vibrational analysis (producing only one imaginary frequency), at the UHF/6-311++G(d,p) level of theory. In addition, the minima connected by a given TS were

confirmed by intrinsic reaction coordinate (IRC) calculations [29], with the UHF/6-31G(d) method/basis.

3. Results and discussion

3.1. Mass spectrometry

All the compounds were studied under EI conditions. The mass spectra of the compounds examined are summarized in Table 2. The molecular ion of all the compounds were observed, but some of them with very low abundance. The fragmentation sequences were clarified by linked scans at constant B/E [30]. Besides mass spectrometric methods, isotopic labelling of benzyl azide was useful for the understanding of some mechanisms.

A metastable transition study was required in order to distinguish between ions resulting from the ionization of thermal degra-

dation products and ions produced by ionization of samples and their further fragmentation. All the fragmentation pathways proposed have been based on both, fragmentation sequences observed in the linked scan spectra and high resolution mass spectra data. In addition, the full optimized structures of the methylbenzyl azide radical cations (2-MBA$^{+\bullet}$, 3-MBA$^{+\bullet}$ and 4-MBA$^{+\bullet}$) were obtained at the UHF/6-311++G(d,p) level. Fig. 1 shows these structures, with special emphasis to changes in the CC-NN dihedral angle, before and after the loss of an electron. In all normal EI spectra intense peaks were detected at m/z 18 being, probably, due to water present in the hygroscopic azides.

3.1.1. Benzyl azide

Although aliphatic azides such as α-carbonyl azides [18] normally lose N_2, from the molecular ion, this was not observed for benzyl azide. It was found, through linked scans at constant B/E, that N_3 and HN_2 were the preferred losses from the molecular ion of benzyl azide (Table 3). The loss of N_3 seems to be the most favoured one (Table 2) since ion at m/z 91 is the base peak. Similar behaviour is observed in a typical EI mass spectrum obtained for deuterated benzyl azide (Fig. 2).

Table 2
EI (70 eV) mass spectra of compounds **1–5**. Relative ionic abundances in %.

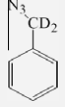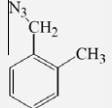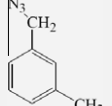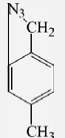| m/z	Compound				
	1	**2**	**3**	**4**	**5**
17	5.0	3.6	5.0	4.0	–
18	24.7	12.9	24.0	19.0	4.2
26	1.0	–	2.0	–	–
27	2.8	2.9	5.0	8.0	1.4
28	34.4	20.0	35.0	31.0	14.8
32	6.3	5.7	5.0	4.0	2.3
37	1.6	2.1	2.0	–	–
38	2.8	2.9	4.0	4.0	–
39	6.9	6.4	18.0	19.0	3.8
40	–	5.0	3.0	4.0	–
41	2.5	2.9	5.0	4.0	1.1
43	1.9	–	2.0	–	–
50	9.4	11.4	7.0	–	1.7
51	16.9	20.7	13.0	8.0	3.0
52	9.1	8.6	5.0	15.0	–
53	–	6.4	4.0	8.0	–
59	–	–	7.0	8.0	–
62	1.6	2.9	5.0	8.0	1.1
63	3.8	4.3	13.0	15.0	2.6
64	1.3	4.3	5.0	8.0	1.0
65	5.9	4.3	22.0	23.0	5.5
66	–	5.7	3.0	4.0	–
67	–	5.7	–	–	–
74	3.1	4.3	2.0	2.0	–
75	2.5	3.6	2.0	2.0	–
76	5.0	5.7	2.0	2.0	–
77	34.4	27.1	13.0	15.0	2.7
78	15.6	8.6	7.0	8.0	1.0
79	1.9	17.1	9.0	8.0	1.8
80	–	4.3	–	–	–
89	1.9	–	13.0	12.0	2.5
90	1.3	2.1	9.0	8.0	1.9
91	100.0	2.9	64.0	77.0	43.6
92	6.3	3.6	15.0	15.0	3.4
93	–	100.0	2.0	–	–
94		9.3			
103	4.1	11.4	8.0	8.0	1.6
104	37.5	8.6	73.0	8.0	1.4
105	5.3	34.3	100.0	100.0	100.0
106	2.5	9.3	9.0	12.0	3.8
107	–	9.3	–	–	–
115	–	–	7.0	–	–
116	–	–	24.0	8.0	2.0
117	–	–	91.0	12.0	3.4
118	–	–	36.0	58.0	59.1
119	–	–	4.0	31.0	17.0
133	M$^{+\bullet}$43.8	–	–	–	–
134	3.8	–	–	–	–
135	–	M$^{+\bullet}$45.7	–	–	–
136	–	5.7	–	–	–
147	–	–	M$^{+\bullet}$15	M$^{+\bullet}$77	M$^{+\bullet}$20.5
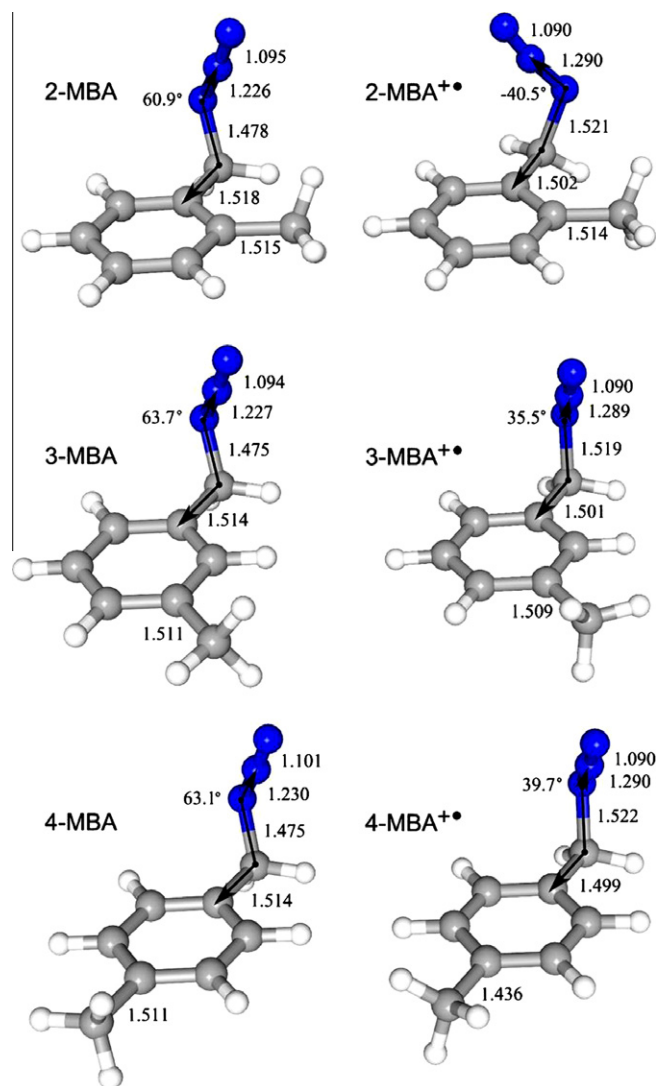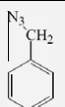
Fig. 1. Optimized structures of 2-, 3- and 4-MBA and corresponding radical cations, obtained with restricted and unrestricted HF/6-311++G(d,p), respectively. Bond lengths are in angstroms (Å).

Table 3
Linked scans data for compounds **1–5**.

Compound	Precursor ion (m/z)	Product ions (m/z)
[structure: N$_3$, CH$_2$, benzene ring]	133 104 91	104, 91 77 65
[structure: N$_3$, CD$_2$, benzene ring]	135 105 93	105, 93 104, 77 67
[structure: N$_3$, CH$_2$, ortho-CH$_3$ ring]	147 118 105 104 91	120, 119, 118, 105, 104 117, 116, 104, 92, 91, 77 104, 103, 79, 78, 77 103, 102, 78, 77 90, 65, 64
[structure: N$_3$, CH$_2$, meta-CH$_3$ ring]	147 118 105 91	119, 118, 117, 105, 91 117, 116, 103, 92, 91, 90, 78, 77 104, 103, 79, 78, 77 90, 65, 64
[structure: N$_3$, CH$_2$, para-CH$_3$ ring]	147 118 105 91	119, 118, 105, 91 92, 91, 77 103, 79, 77 65

Table 4
Accurate mass data for benzyl azide.

m/z	Elemental composition	Measured value	Calculated value	Diff. (ppm)
133	$C_7H_7N_3$	133.06416	133.06400	−1.2
104	C_7H_6N	104.05079	104.05002	−7.4
91	C_7H_7	91.05380	91.05478	10.7
77	C_6H_5	77.03846	77.03913	8.7
65	C_5H_5	65.03786	65.03913	19.4

other main loss, HN$_2$, is also clarified by the deuterated benzyl azide. Since the latter benzyl azide loses DN$_2$ the leaving hydrogen/deuterium is in a neighbouring position relative to the azido group.

3.1.2. Methylbenzyl azides

From the mass spectrometry data analysis it can be concluded that all the methylbenzyl azides present common features. All the normal mass spectra showed the molecular ion peak which is most intense in the case of the *meta*-isomer (see Table 2). The linked scans study was essential to establish sequential fragmentation patterns of benzylic azides. Based on both, linked scans (Table 3) and accurate mass measurements (Table 5), a possible general mechanism for *para*-methylbenzyl azide is summarized in Fig. 4. In this scheme is observed a forbidden transition, loss of HN$_2^\bullet$ from the molecular ion followed by the loss of another radical, CN$^\bullet$. Nevertheless, exceptions to the even electron rule, are reported in the literature [31]. However, when the molecular ion loses 29 Da, the sequential loss of N$_2$ and H cannot be excluded.

Considering benzyl azide as the model compound we found that there should be at least two possible major fragmentation pathways, corresponding to loss of 29 and 42 Da from the molecular ion. These losses must be due to elimination of HN$_2$ radical and N$_3$ radical from the molecular ion. The resulting ions in the case of benzyl azide are at m/z 104 and 91, respectively, and in the cases of all methyl isomers are at m/z 118 and 105.
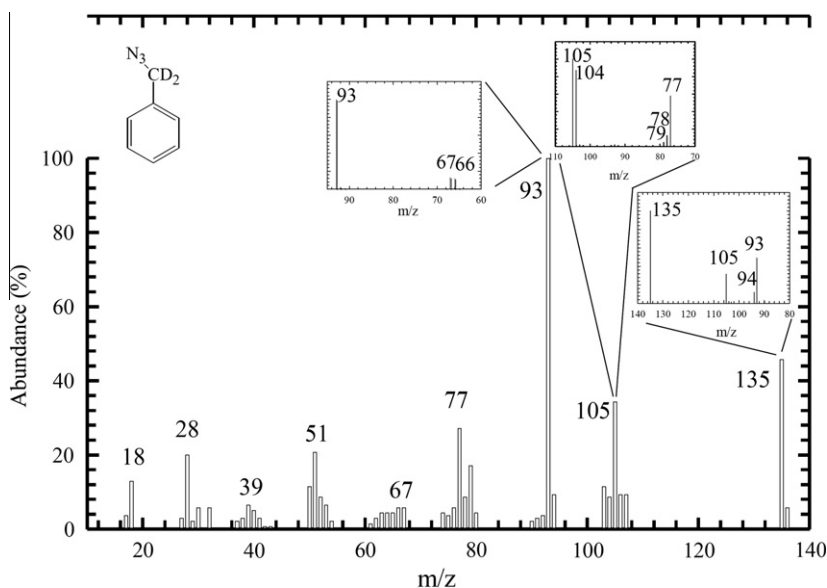
For this azide the peak at m/z 28 can be explained by thermal decomposition prior to ionization. From Table 3 it can be seen that the molecular ion never loses 28 Da.

The fragmentation mechanisms were established by linked scans at constant B/E and accurate mass measurements (Tables 3 and 4). The proposed mechanisms were supported by labelling as presented in Fig. 3. According with the parallel mechanisms, in that figure, the ion at m/z 91 and its deuterated form at m/z 93 must have a tropylium ion structure. In fact, ion at m/z 93 displays a loss of C_2H_2 and not C_2D_2 which proves a scrambling of H/D atoms only possible in a $C_7H_7^+$ with a tropylium structure. Furthermore, the

Fig. 2. Mass spectrum for deuterated benzyl azide and its linked scan at constant B/E for the main peaks.
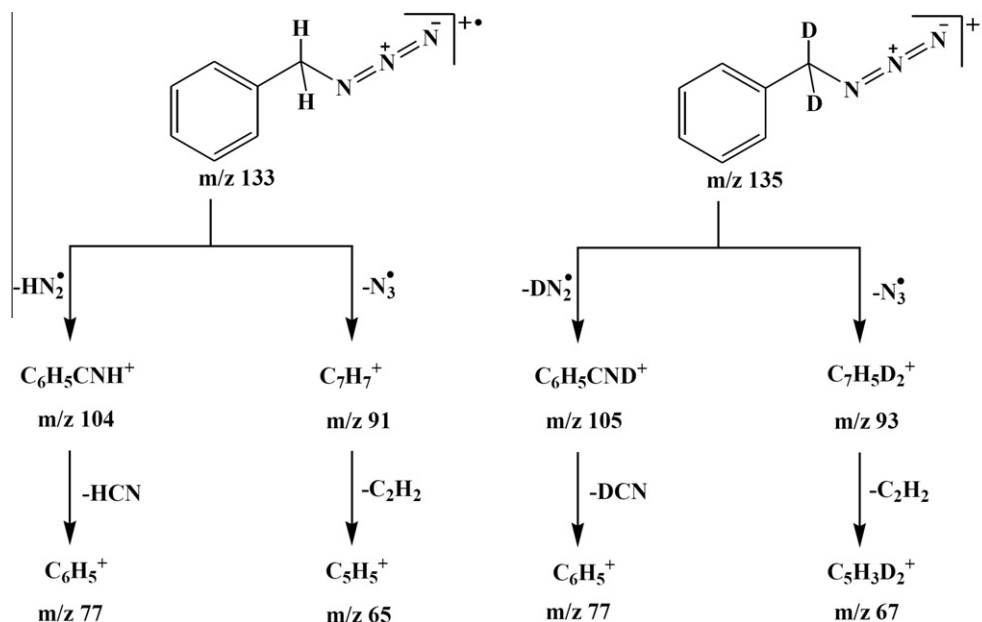
Fig. 3. Main fragmentation pathways, for benzyl azide and deuterated benzyl azide, based on metastable transitions and accurate mass measurements.

Table 5
Accurate mass data for *para*-methylbenzyl azide.

m/z	Elemental composition	Measured value	Calculated value	Diff. (ppm)
147	$C_8H_9N_3$	147.07938	147.07965	1.8
119	C_8H_9N	119.07274	119.07350	6.4
118	C_8H_8N	118.06627	118.06567	−5.0
105	C_8H_9	105.07055	105.07043	−1.2
103	C_8H_7	103.05347	103.05478	12.6
92	C_7H_8	92.06064	92.06260	21.3
91	C_7H_7	91.05582	91.05478	−11.5
79	C_6H_7	79.05639	79.05478	−20.5
77	C_6H_5	77.04060	77.03913	−19.1
65	C_5H_5	65.03960	65.03913	−7.3

Among all methyl isomers the *ortho* can be characterized by a very abundant ion at m/z 104. In fact, the presence of a CH_3 group

in the *ortho* position must be a determinant factor for the releasing of HN_3 from the molecular ion. This metastable transition is not observed for the other isomers, which explains the insignificant abundance of ion at m/z 104 in the other two isomers. On the other hand, while there is a parallel between the mechanism that leads to the formation of ion at m/z 118 in methylbenzyl azides and the formation of an ion at m/z 104 for benzyl azide, the ion at m/z 104 for *ortho*-methylbenzyl azide must be formed through a different mechanism, involving a six member ring intermediate (Fig. 5), not observed for the other isomers neither for benzyl azide.

Another interesting difference of the *ortho*-isomer towards the *meta*- and *para*-isomers is the origin of ion at m/z 91. This ion has various precursor ions as shown in Table 3. For *meta*- and *para*-isomers this ion can be a product ion of the molecular ion by loss of $CH_2N_3^\bullet$ unlike the *ortho* for which this route is not observed. This is consistent with a favoured loss of HN_3 from the
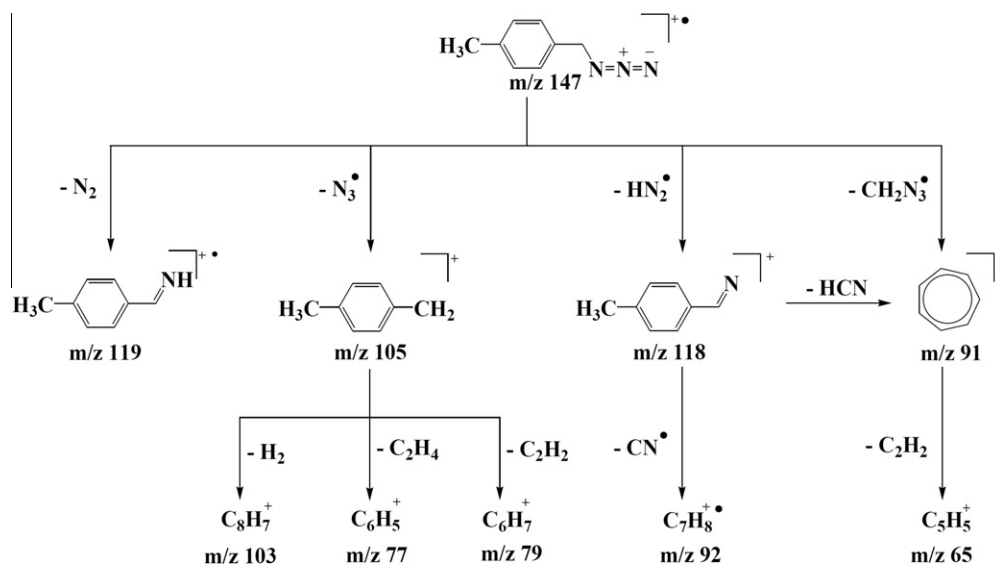

Fig. 4. Main fragmentation pathways, for *para*-methylbenzyl azide, based on metastable transitions and accurate mass measurements.
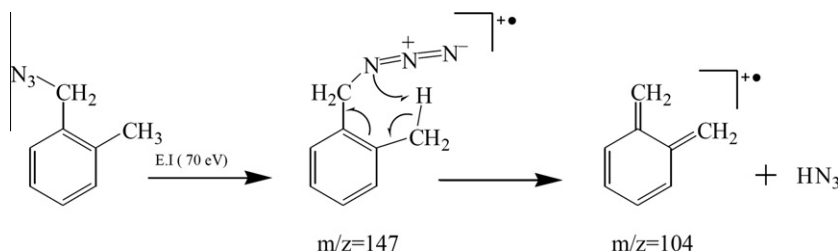
Fig. 5. Possible mechanism for formation of ions at m/z 104 in *ortho*-methylbenzyl azide.

molecular ion in the *ortho* case. This is an example of the reported *ortho* effect [32,33] which explains rearrangements involving hydrogen transfer between neighbouring groups on an aromatic ring. A rigid planar arrangement of the interacting groups facilitates the formation of a cyclic transition state. This effect is very useful in the characterization of *ortho*-substituted compounds as the larger spatial separation of interacting groups, in *meta*- and *para*-substituted isomers, makes the same type of interaction weaker or nonexistent.

The main difference between *meta*- and *para*-isomers is that less fragmentation is observed in the normal spectra, for the *para* isomer, which is supported by a smaller number of metastable transitions (Table 3). In fact, the substituents in *para* position must introduce resonance stabilization in the resulting ions. Moreover, comparing *meta* and *para* fragmentations, from the linked scans in Table 3, it can be seen that besides the fragmentation routes presented in Fig. 4 for *para*, some other complementary routes can be observed for *meta*, namely the fragmentation routes for ions at m/z 105 and 91. Nevertheless, the *meta* derivative presents the most abundant molecular ion. This must be due to the methyl group in *meta* position not being able to stabilize positive charges of the fragments. In addition, the abundance of ion at m/z 91 is higher for *meta* isomer.

Finally, in spite of the strong evidence of its occurrence in the linked scans results, the first two pathways presented in Fig. 4 were also confirmed by IRC calculations. The route leading to the formation of *para*-methyl-benzylidene imine cation, through N_2 elimination and concerted migration of the H atom to the neighbouring N, is depicted in Fig. 6, where a reaction barrier of approximately 33.9 kJ/mol was computed at the UHF/6-31G(d) level of

theory. The TS is formed by a concerted mechanism: simultaneous to the elongation of the $N-N_2$ bond, the $H-C-N$ angle closes significantly.

The second pathway portrayed in Fig. 4, releasing of N_3 from the *para*-isomer, and formation of the N_3 radical plus the *para*-methylbenzyl cation, has also been the subject of theoretical investigation. IRC calculations initiated at the transition structure connecting the precursor ion and product molecules are shown in Fig. 7, where a reaction barrier of approximately 19.5 kJ/mol arises. This barrier lower than the one for the N_2 loss explains the m/z 105 ion abundance higher than the one for m/z 119 ion (Table 2). In addition, for benzyl azide, the $N_3^\bullet$ elimination must be, also, the most favoured decomposition channel as m/z 91 corresponds to the most abundant ion.

Table 6 presents the total and relative energies of benzyl azide and methylbenzyl azide radical cations, as well as transition struc-
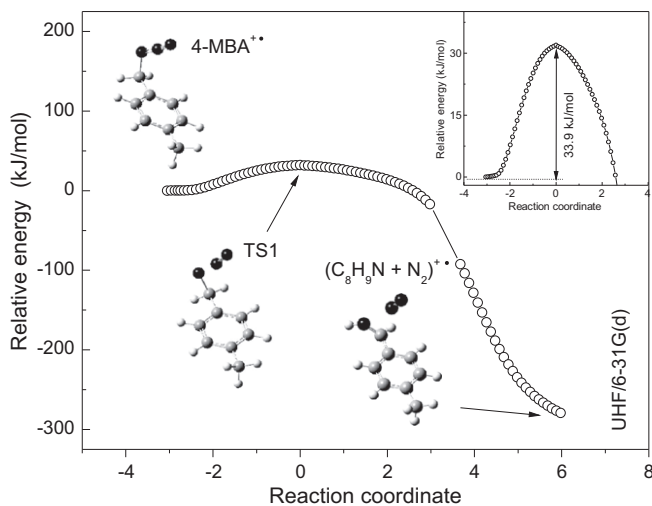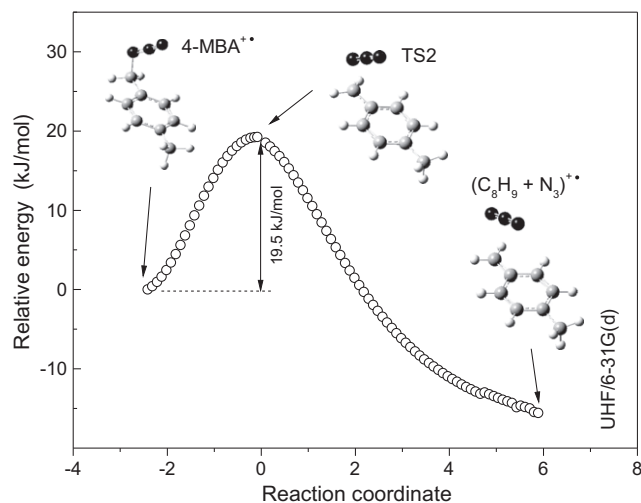

Fig. 7. IRC calculation results for the fragmentation pathway leading to the formation of *para*-methylbenzyl cation + N_3 radical from 4-MBA$^{+\bullet}$, determined with UHF/6-31G(d).

Table 6
Total (hartree) and relative energies (kJ/mol) of benzyl and methylbenzyl azide ions, selected transition structures and corresponding fragmentation products.

Cations	UHF/6-311++G(d,p)	
	Total energy	Relative energy
BA$^{+\bullet}$	−432.233760	–
2-MBA$^{+\bullet}$	−471.279870	–
3-MBA$^{+\bullet}$	−471.282090	–
4-MBA$^{+\bullet}$	−471.283047	0
TS1$^+$	−471.272439	27.85
TS2$^+$	−471.275500	19.81
$(C_8H_9N+N_2)^{+\bullet}$	−471.293263	−341.97
$(C_8H_9+N_3)^{+\bullet}$	−471.293263	−26.82

Fig. 6. IRC calculation results for the fragmentation pathway leading to the formation of *para*-methylbenzylidene imine radical cation + N_2 from 4-MBA$^{+\bullet}$, determined with UHF/6-31G(d).

tures and fragmentation products associated with the first two channels depicted in Fig. 4, obtained at UHF/6-311++G(d,p) level. The fully optimized transition structures TS1 and TS2, also obtained with UHF/6-311++G(d,p), are shown in Fig. 8, where some selected geometric parameters are emphasized. Resuming the frag-
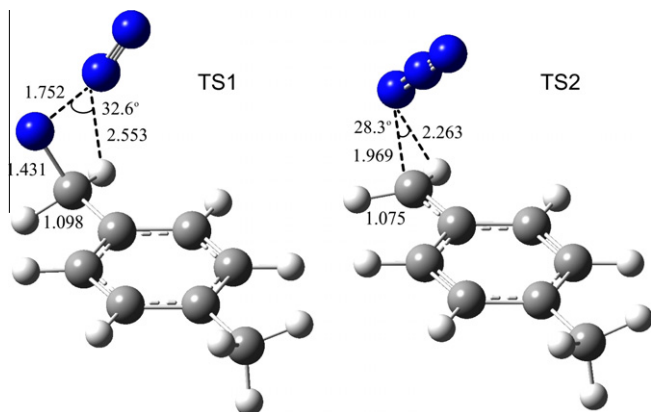

Fig. 8. Optimized structures of TS1 and TS2, connecting 4-MBA$^{+\bullet}$ and the products from the first two fragmentation channels of Fig. 4, obtained with UHF/6-311++G(d,p). Bond lengths and distances are in angstroms (Å).
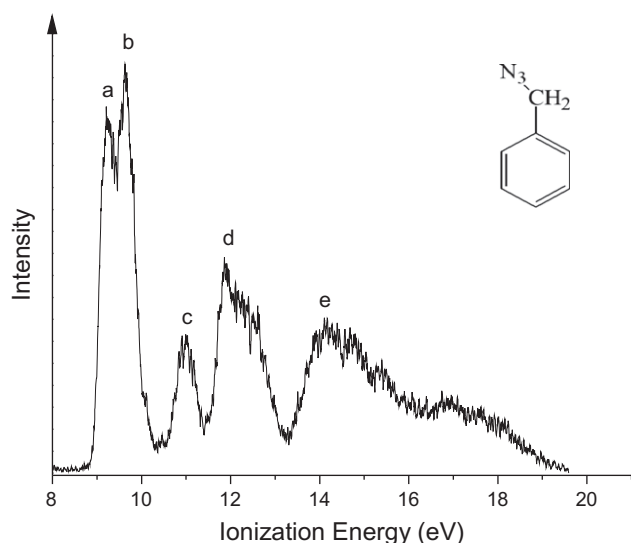

Fig. 9. He(I) photoelectron spectrum of benzyl azide. The labeled bands are listed in Table 7.

mentation routes in Fig. 4, two of them were not investigated, by IRC calculations, $CH_2N_3^{\bullet}$ and $HN_2^{\bullet}$ elimination. The former pathway, loss of $CH_2N_3^{\bullet}$, yielded $C_7H_7^+$, which must present a tropylium ion structure. For the latter loss, HN_2, it is expected that the experimental evidence obtained for benzyl azide, shown in Fig. 3, applies. This means that the release of HN_2 must involve an hydrogen from the $-CH_2-$ group adjacent to the azido group.

3.2. Photoelectron spectroscopy

Assignment of He(I) PE spectra of benzyl azide and methylbenzyl azides was made with reference to our recent results on *ab initio* molecular orbital calculations [34]. Results arising from calculations with the HF method and the 6-311++G(d,p) basis provide a good qualitative description of the MOs shapes and orientations. For each azide, the PE spectra were recorded, and experimental vertical ionization energies (VIEs) were obtained by averaging the VIEs of the bands from several different spectra. Typical PE spectra and MOs for theses azides are shown in Figs. 9–11a–c. Experimental and calculated VIEs are summarized in Tables 7 and 8.

3.2.1. Benzyl and methylbenzyl azides

Fig. 9 shows a typical PE spectrum, at room temperature, of benzyl azide. Five distinct bands labeled a–e in this figure may be readily identified. The shapes and orientations of the MOs of BA resulting from calculations with the HF method and the 6-311++G(d,p) basis are presented in Fig. 10. Experimental and calculated VIEs of the benzyl azide are listed in Table 7, where a quite satisfactory agreement between the calculated values and the experimental data is clearly seen.

The first two intense bands of the BA photoelectron spectrum (see Fig. 9 and Table 7), at 9.28 and 9.63 eV, respectively, can be assigned to the two highest occupied MOs in the ground state of this molecule, originated mainly from the degenerate $1e_{1g}$ HOMO of benzene [35], which follows either a π_2 (HOMO) or a π_3 (MO 34) pattern. The bands centered at 10.96 and 11.88 eV can be attributed to MOs coming from the azido group N_3: the third (MO 33) is comprised almost exclusively from the $\pi_{N_3}^*$ MO established in the nitrogen chain, whereas the fourth (MO 32) is a $\sigma_{N_3}^*$ that also features a very small σ_{CN} contribution. Considering the three outermost orbitals, $(11a')(12a')(3a'')$, in the electronic configuration of methyl azide, CH_3N_3 [36], one can undoubtedly relate the third MO to the $3a''$ state of CH_3N_3 and the fourth MO to the $12a'$ state of CH_3N_3.
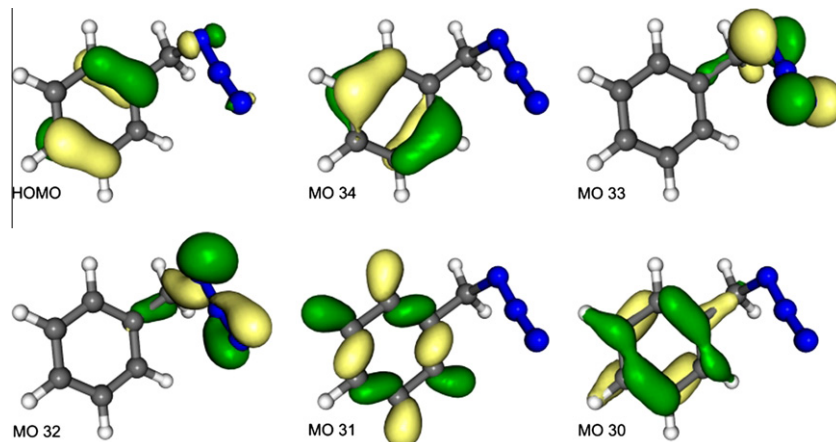

Fig. 10. Selected molecular orbitals (HOMO-MO 30) from benzyl azide, based on HF/6-311++G(d,p) results.
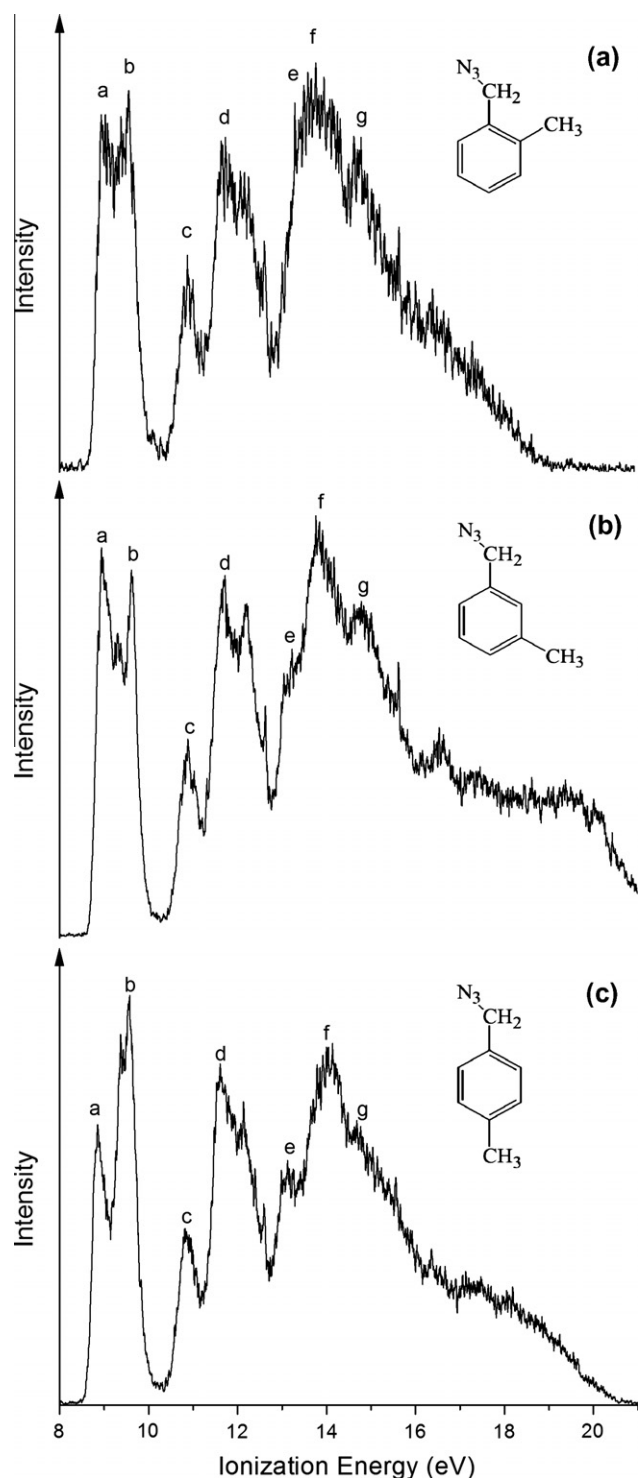
Fig. 11. He(I) photoelectron spectra obtained for: (a) *ortho*-methylbenzyl azide; (b) *metha*-methylbenzyl azide; and (c) *para*-methylbenzyl azide. The labeled bands are listed in Table 8.

Table 7

Experimental (VIE) and calculated (-ϵ_i) ionization energies (eV) of benzyl azide. ΔE and MO stands for experimental energy uncertainty and molecular orbital, respectively.

Experimental			Calculated	
Band	VIE	ΔE	MO	$-\epsilon_i$
a	9.28	0.01	HOMO	9.26
b	9.63	0.01	34	9.44
c	10.96	0.01	33	10.36
d	11.88	0.04	32	12.03
			31	13.67
e	14.13	0.09	30	13.78
			29	14.06

MBA) and *para*-methylbenzyl azide (4-MBA). Seven bands labeled a–g may be identified, respectively, in this figure. The photoelectron spectra also show traces of water (12.62 eV) [24], due to the samples' hygroscopic nature. Experimental and calculated VIEs of 2-, 3- and 4-MBA are listed in Table 8, which also shows a satisfactory agreement between the calculated values and the experimental data.

Bands a and b in the PE spectra of the BA methyl derivatives (Fig. 11a–c) can also be related to two patterns of the degenerate 1e$_{1g}$ HOMO of benzene. Bands c and d can be attributed to the third and fourth MOs of 2-, 3- and 4-MBA, that also come from the azido group N$_3$: a $\pi^*_{N_3}$ MO and a σ_{N_3} MO, respectively. In a similar way to the BA spectrum, band e in the PE spectrum of the methylbenzyl azides results from the overlap of several benzene orbitals. Finally, band f is associated with another π pattern of 3e$_{2g}$ of benzene.

4. Conclusions

Benzyl azide and its methyl substituted isomers have been synthesized and characterized by mass spectrometry and UV photoelectron spectroscopy.

Mass spectrometry allowed us to examine the fragmentation pathways of benzyl azide and to investigate the effect of different relative positions of methyl group, on the aromatic ring, on the fragmentation of the benzyl azides. The N$_3^{\bullet}$ loss is favoured in all five compounds. In addition, theoretical calculations showed that in terms of barriers for N$_3^{\bullet}$ and N$_2$ elimination channels, the former is more favourable. The loss of C$_2$H$_2$ from the fragment m/z 105 can be expected via a pericycle reaction involving a 1,2 hydrogen migration, which is helped by the electronic effect of the methyl group. The application of mass spectrometry techniques proved to be effective, in particular, in characterization and differentiation of the *ortho*-isomer. In fact, the substituent group in the *ortho* position has a profound influence on the fragmentation pathways and consequently on the ion abundance. The differentiation between *meta*- and *para*-isomers is not so unequivocally established as for *ortho*. However, some evidence to distinguish them was observed.

The He(I) photoelectron spectra of 2-MBA, 3-MBA and 4-MBA and the He(I) photoelectron spectrum of BA are quite similar within the 8–13 eV ionization energy range. The molecular orbital calculations, concerning the four existing bands in that region, show two bands below 10 eV associated with π benzene ring orbitals, while above that energy, the other two bands are associated with the azide chain orbitals. Moving towards the 13–16 eV ionization energy range, the BA presents a broad band while three bands arise for their methyl derivatives. According to the theoretical calculations, and in contrast with former experimental results on aliphatic azides, the HOMO ionization energy is associated with removal of an electron from a MO located on the benzene ring and not on the azido group.

The broad band e arises from overlap of the remaining MOs and correspond chiefly to several benzene orbitals, with more or less contributions from the nitrogens. MO 31 portraits a strong resemblance to the degenerate 3e$_{2g}$ orbital (σ) of benzene. MO 30 is mainly constituted from benzene's 1a$_{2u}$ orbital, following a π_1 pattern.

Fig. 11a–c shows typical PE spectra, at room temperature, of *ortho*-methylbenzyl azide (2-MBA), *meta*-methylbenzyl azide (3-

Table 8
Experimental (VIE) and calculated ($-\epsilon_i$) ionization energies (eV) of *ortho*-methylbenzyl azide, *metha*-methylbenzyl azide and *para*-methylbenzyl azide. ΔE and MO stands for experimental energy uncertainty and molecular orbital, respectively.

Band	2-MBA			3-MBA			4-MBA			
	Experimental		Calc.	Experimental		Calc.	Experimental		Calc.	
	VIE	ΔE	$-\epsilon_i$	VIE	ΔE	$-\epsilon_i$	VIE	ΔE	$-\epsilon_i$	MO
a	9.03	0.02	9.09	9.02	0.01	8.99	8.89	0.01	8.95	HOMO
b	9.47	0.04	9.20	9.61	0.01	9.31	9.50	0.01	9.36	38
c	10.88	0.01	10.30	10.88	0.01	10.30	10.88	0.01	10.28	37
d	11.84	0.08	11.98	11.69	0.02	11.98	11.66	0.02	11.96	36
e	13.36	0.13	13.42	13.16	0.02	13.41	13.14	0.03	13.41	35
			13.47			13.45			13.47	34
f	13.72	0.09	13.76	13.87	0.02	13.82	14.08	0.02	13.74	33
g	14.71	0.05	15.04	14.75	0.01	14.83	14.69	0.04	14.79	32

References

[1] G. L'Abbé, Chem. Rev. 69 (1969) 345–363.
[2] E.F.V. Scriven, K. Turnbull, Chem. Rev. 88 (1988) 297–368.
[3] S.B. se, C. Gil, K. Knepper, V. Zimmermann, Angew. Chem., Int. Ed. 44 (2005) 5188–5240.
[4] P.L. Golas, N.V. Tsarevsky, K. Matyjaszewski, Macromol. Rapid Commun. 29 (2008) 1167–1171.
[5] G.O. Jones, K.N. Houk, J. Org. Chem. 73 (2008) 1333–1342.
[6] D.P. Nguyen, H. Lusic, H. Neumann, P.B. Kapadnis, A. Deiters, J.W. Chin, J. Am. Chem. Soc. 131 (2009) 8720–8721.
[7] F. Amblard, J.H. Cho, R.F. Schinazi, Chem. Rev. 109 (2009) 4207–4220.
[8] Y. Song, J.M. Chan, Z. Tovian, A. Secrest, E. Nagy, K. Krysiak, K. Bergan, M.A. Parniak, E. Oldfield, Bioorg. Med. Chem. 16 (2008) 8959–8967.
[9] J.A. Prescher, D.H. Dube, C.R. Bertozzi, Nature 430 (2004) 873–877.
[10] A.B. Smith, I.G. Safonov, R.M. Corbett, J. Am. Chem. Soc. 124 (2002) 11102–11113.
[11] Q.S. Li, H.X. Duan, J. Phys. Chem. A 109 (2005) 9089–9094.
[12] E.W. Meijer, S. Nijhuis, F.C.B.M.V. Vroonhoven, J. Am. Chem. Soc. 110 (1988) 7209–7210.
[13] H. Niino, T. Sato, A. Yabe, Appl. Phys. A: Mater. Sci. Process. 69 (1999) 145–148.
[14] J.M. Dyke, A.P. Groves, A. Morris, J.S. Ogden, A.A. Dias, A.M.S. Oliveira, M.L. Costa, M.T. Barros, M.H. Cabral, A.M.C. Moutinho, J. Am. Chem. Soc. 119 (1997) 6883–6887.
[15] J.M. Dyke, A.P. Groves, A. Morris, J.S. Ogden, M.I. Catarino, A.A. Dias, A.M.S. Oliveira, M.L. Costa, M.T. Barros, M.H. Cabral, A.M.C. Moutinho, J. Phys. Chem. A 103 (1999) 8239–8245.
[16] N. Hooper, L.J. Beeching, J.M. Dyke, A. Morris, J.S. Ogden, A.A. Dias, M.L. Costa, M.T. Barros, M.H. Cabral, A.M.C. Moutinho, J. Phys. Chem. A 106 (2002) 9968–9975.
[17] R.T.M. Fraser, N.C. Paul, M.J. Bagley, Org. Mass Spectrosc. 7 (1973) 83–88.
[18] M.F. Duarte, F. Martins, M.T. Fernandez, G.J. Langley, P. Rodrigues, M.T. Barros, M.L. Costa, Rapid Commun. Mass Spectrom. 17 (2003) 957–962.
[19] F. Martins, M.F. Duarte, M.T. Fernandez, G.J. Langley, P. Rodrigues, M.T. Barros, M.L. Costa, Rapid Commun. Mass Spectrom. 18 (2004) 363–366.
[20] M. Barros, M. Beyer, M. Costa, M. Duarte, M. Fernandez, F. Martins, P. Rodrigues, P. Watts, Int. J. Mass Spectrom. 237 (2004) 65–73.
[21] E.A. Betterton, Crit. Rev. Environ. Sci. Technol. 33 (2003) 423–458.
[22] S.G. Alvarez, M.T. Alvarez, Synthesis 1997 (1997) 413–414.
[23] A. Morris, N. Jonathan, J.M. Dyke, P.D. Francis, N. Keddar, J.D. Mills, Rev. Sci. Instrum. 55 (1984) 172–181.
[24] K. Kimura, Handbook of HeI photoelectron spectra of fundamental organic molecules: ionization energies, ab initio assignments, and valence electronic structure for 200 molecules, Japan Scientific Societies Press, Halsted Press, Tokyo, New York, 1981.
[25] M.J. Frisch, G.W. Trucks, H.B. Schlegel, G.E. Scuseria, M.A. Robb, J.R. Cheeseman, J.A. Montgomery Jr., T. Vreven, K.N. Kudin, J.C. Burant, J.M. Millam, S.S. Iyengar, J. Tomasi, V. Barone, B. Mennucci, M. Cossi, G. Scalmani, N. Rega, G.A. Petersson, H. Nakatsuji, M. Hada, M. Ehara, K. Toyota, R. Fukuda, J. Hasegawa, M. Ishida, T. Nakajima, Y. Honda, O. Kitao, H. Nakai, M. Klene, X. Li, J.E. Knox, H.P. Hratchian, J.B. Cross, V. Bakken, C. Adamo, J. Jaramillo, R. Gomperts, R.E. Stratmann, O. Yazyev, A.J. Austin, R. Cammi, C. Pomelli, J.W. Ochterski, P.Y. Ayala, K. Morokuma, G.A. Voth, P. Salvador, J.J. Dannenberg, V.G. Zakrzewski, S. Dapprich, A.D. Daniels, M.C. Strain, O. Farkas, D.K. Malick, A.D. Rabuck, K. Raghavachari, J.B. Foresman, J.V. Ortiz, Q. Cui, A.G. Baboul, S. Clifford, J. Cioslowski, B.B. Stefanov, G. Liu, A. Liashenko, P. Piskorz, I. Komaromi, R.L. Martin, D.J. Fox, T. Keith, M.A. Al-Laham, C.Y. Peng, A. Nanayakkara, M. Challacombe, P.M.W. Gill, B. Johnson, W. Chen, M.W. Wong, C. Gonzalez, J.A. Pople, Gaussian 03, Revision C.02, Gaussian, Inc., Wallingford, CT, 2004.
[26] R. Krishnan, J.S. Binkley, R. Seeger, J.A. Pople, J. Chem. Phys. 72 (1980) 650–654.
[27] J.P. Santos, M.L. Costa, R.I. Olariu, F. Parente, Eur. Phys. J. D 39 (2006) 379–384.
[28] T. Koopmans, Physica 1 (1934) 104–113.
[29] C. Gonzalez, H.B. Schlegel, J. Phys. Chem. 94 (1990) 5523–5527.
[30] A.P. Bruins, K.R. Jennings, S. Evans, Int. J. Mass Spectrom. Ion Process. 26 (1978) 395–404.
[31] M. Karni, A. Mandelbaum, Org. Mass Spectrosc. 15 (1980) 53–64.
[32] H. Schwarz, Organic Chemistry Topics in Current Chemistry, Springer, Berlin/Heidelberg, 1978.
[33] D. Blachut, W. Danikiewicz, M. Olejnik, Z. Czarnocki, J. Mass Spectrom. 39 (2004) 966–972.
[34] R.M. Pinto, A.A. Dias, M.L. Costa, J.P. Santos, J. Mol. Struct.: Theochem. 948 (2010) 15–20.
[35] V.G. Zakrzewski, J.V. Ortiz, J. Phys. Chem. 100 (1996) 13979–13984.
[36] H. Bock, R. Dammel, J. Am. Chem. Soc. 110 (1988) 5261–5269.